ACS OMEGA

http://pubs.acs.org/journal/acsodf

Article

Enhanced Catalytic Activity of a New Nanobiocatalytic System Formed by the Adsorption of Cytochrome *c* on Pluronic Triblock Copolymer Stabilized MoS_2 Nanosheets

Anu Maria Chittilappilly Devassy, Adithya Kamalakshan, Nidhi Anilkumar Jamuna, Roselin Ansilda, and Sarthak Mandal*

Cite This: *ACS Omega* 2022, 7, 16593−16604

Read Online

ACCESS | Metrics & More | Article Recommendations | Supporting Information

ABSTRACT: The formation of nanobiohybrids through the immobilization of enzymes on functional nanomaterials has opened up exciting research opportunities at the nanobiointerfaces. These systems hold great promise for a wide range of applications in biosensing, biocatalytic, and biomedical fields. Here, we report the formation of a hybrid nanobiocatalytic system through the adsorption of cytochrome *c* (Cyt *c*) on pluronic triblock copolymer, P123 (PEO-*b*-PPO-*b*-PEO), stabilized MoS_2 nanosheets. The use of pluronic polymer has helped not only to greatly stabilize the exfoliated MoS_2 nanosheets but also to allow easy adsorption of Cyt *c* on the nanosheets without major structural changes due to its excellent biocompatibility and soft protein-binding property. By comparing the catalytic activity of the Cyt *c*−MoS_2 nanobiohybrid with that of the free Cyt *c* and as-prepared MoS_2 nanosheets, we have demonstrated the active role of the nanobiointeractions in enhancing the catalytic activity of the hybrid. Slight structural perturbation at the active site of the Cyt *c* upon adsorption on MoS_2 has primarily facilitated the peroxidase activity of the Cyt *c*. As the MoS_2 nanosheets and the native Cyt *c* individually exhibit weaker intrinsic peroxidase activities, their mutual modulation at the nanobiointerface has made the Cyt *c*−MoS_2 a novel nanobiocatalyst with superior activity.

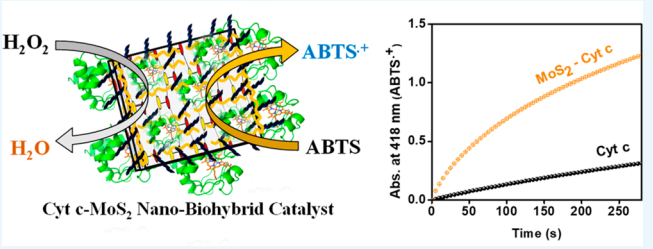

1. INTRODUCTION

The discovery of a two-dimensional (2D) layered graphene nanomaterial opened up an area of intensive research due to its exceptional mechanical strength, high thermal and electrical conductivity, and optical properties.[1−4] Since then, graphene-like 2D nanosheet materials such as transition metal dichalcogenides (TMDCs), graphitic carbon nitride, MXenes, hexagonal boron nitride (h-BN), and transition metal oxides (TMOs) have become the center of attention.[5] 2D layered materials (single or few layers) are more fascinating than their bulk form because of the high density of active surface sites available over a large area.[6] A broad range of electronic properties like metallic/semimetallic (e.g., graphene, VS_2, TaS_2) to semiconducting (e.g., MoS_2, WS_2) or insulating (e.g., h-BN) properties are exhibited by them.[4,5] Similarly, they have a broad range of optical properties like fluorescence quenching or emission behavior.[7,8] 2D molybdenum disulfide (MoS_2) is one of the pioneers of TMDC materials with an excellent layer-dependent band structure.[9,10] A direct band gap of ∼1.8 eV possessed by the monolayer MoS_2 nanosheet makes it a good semiconducting material, resolving the gapless problems of graphene.[11] A single MoS_2 nanosheet is composed of a layer of Mo atoms sandwiched between two layers of S atoms. Strong covalent bonding between Mo and S atoms strengthens the trilayer MoS_2 nanosheet, and a weak Van der Waal force stacks them up. The MoS_2 nanosheet can have two distinct crystalline phases at room temperature, one with trigonal prismatic coordination, which is found to be semiconducting (2H), and the other one with octahedral coordination (1T), which is metallic.

MoS_2 nanosheets have gained burgeoning interest in biosensor, biocatalytic and biomedical applications specifically due to their unique optoelectronic properties, high capacity of biomolecule loadings and good biocompatibility.[12−19] Moreover, their tailoring behavior to selectively respond to specific analytes with high sensitivity through different surface functionalizations has led to their extensive usage in biosensing and biocatalytic applications.[20,21] Although natural enzymes can perform catalytic activity with high efficiency and selectivity, they often require strict reaction conditions like specific temperature, pH, and ionic strength. The instability of natural enzymes under drastic conditions limits their industrial

Received: February 10, 2022
Accepted: April 15, 2022
Published: May 3, 2022

Scheme 1. Schematic Illustration of the Formation of the Cyt *c*−MoS_2 Nanobiocatalyst by the Spontaneous Adsorption of Cyt *c* on Triblock Copolymer, P123, Stabilized MoS_2 Nanosheets[a]

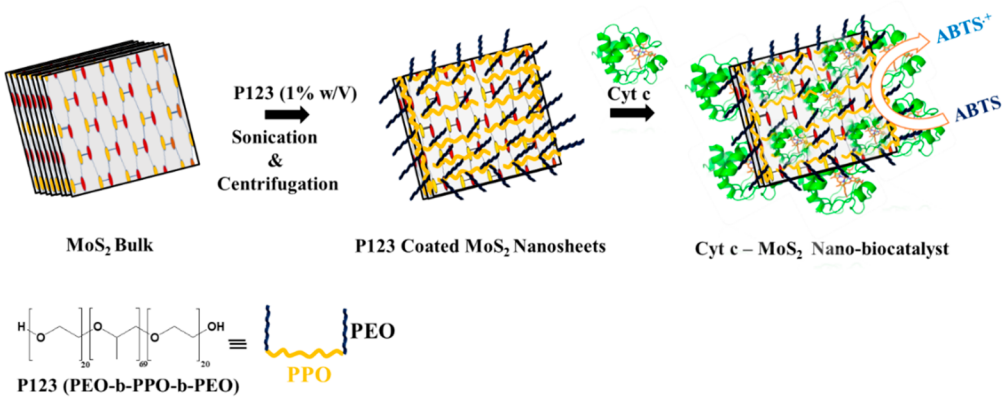

[a]The oxidation of ABTS by the nanobiocatalyst in the presence of H_2O_2 has been used to demonstrate its enhanced peroxidase-like catalytic activity.

applications.[22] To overcome these limitations, researchers are now focusing on the development of new low-cost, stable, and active nanobiocatalytic systems by interfacing natural proteins/enzymes on a wide variety of functional nanomaterials (or nanozymes).[23] In this work, we have demonstrated superior catalytic performance of a new Cyt *c*−MoS_2 nanobiocatalytic system developed by interfacing Cyt *c* on triblock copolymer P123 stabilized MoS_2 nanosheets (Scheme 1).

The MoS_2 nanosheets used in this work were synthesized via the ultrasonication-assisted liquid-phase exfoliation method.[10] This method provides a simple but effective route for obtaining sufficient quantities of thin-layered MoS_2 nanosheets with high structural quality. This method has previously been extensively employed using various types of surfactants and polymers as dispersants to yield MoS_2 nanosheets/nanoparticles of varying sizes and thicknesses.[10,24,25] Here we have used 1% (w/v) aqueous solution of a pluronic triblock copolymer, P123, as an effective dispersant for the exfoliation of bulk MoS_2. P123 is a nonionic amphiphilic triblock copolymer composed of hydrophobic poly(propylene oxide) (PPO) and hydrophilic poly(ethylene oxide) (PEO) blocks. The choice of P123 was made based on the biocompatible nature of the polymer and its preventive role toward aggregation or the major structural change of proteins after adsorption on nanomaterials.[26] The large molecular weight of the polymer and its long hydrophobic and hydrophilic chains also provides effective stabilization to the exfoliated MoS_2 nanosheets by capping on their surface. The hydrophobic PPO units can be adsorbed on the MoS_2 nanosheets, while the hydrophilic PEO polymer chains remain extended into the bulk solution (Scheme 1). These hydrophilic chains provide effective steric hindrance to prevent flocculation or aggregation of the nanosheets.[27−30] Apart from providing a biocompatible environment, the polymer chains on MoS_2 nanosheets also play an important role in anchoring more Cyt *c* on the nanosheets for enhanced catalytic activity of the hybrid.

Cytochrome *c* (Cyt *c*) is a globular heme protein which functions as an electron carrier for oxidative phosphorylation (or mitochondrial respiration) in the inner mitochondrial membrane of healthy cells.[31,32] The Fe center of Cyt *c* is six coordinated in its native state with methionine (Met 80) as a distal ligand.[33] The protein chain of Cyt *c* consists of 104 amino acids with an isoelectric point of ∼10 (due to the presence of a large number of basic amino acids like lysine). Hence, Cyt *c* bears positive surface charge at physiological pH.[32] Although Cyt *c* primarily functions as an electron carrier in its native state, under pro-apoptotic (programmed cell death) conditions it gains peroxidase activity in the presence of H_2O_2.[31,34,35] Certain conformational change of Cyt *c* induced by its interactions with membrane-bound cardiolipin is believed to be responsible for gaining *in vivo* peroxidase activity.[36] However, the exact nature of the conformation and the mechanism by which it gains peroxidase activity still remain elusive. Classical peroxidases have a five-coordinate heme structure, and the sixth coordination of the iron center is either vacant or occupied by a loosely bound water molecule.[37] This structural feature facilitates the interaction of H_2O_2 with the iron center. Peroxidases generally follow a mechanism in which H_2O_2 reacts with the Fe(III) resting state of heme to produce an oxyferryl compound (Fe(IV)═O heme) known as Compound I along with an adjacent radical. The resting state of enzymes is regenerated with the abstraction of hydrogen from organic substrates, and the newly formed radical then yields stable oxidation products upon reactions with O_2.[34]

The native Cyt *c* becomes a potent peroxidase only after some conformational changes (or after the formation of a partially unfolded structure) with the weakening or rupturing of the Met80 S−Fe bond.[32,34] The improved peroxidase-like catalytic activity of Cyt *c* has been extensively investigated using a wide variety of supporting materials such as polymers,[38] graphene oxide nanosheets,[39,40] metal organic frameworks,[41] carbon dots,[42] and silica nanoparticles.[32] However, no such study has been reported using 2D MoS_2 nanosheets as supporting materials in spite of the outstanding catalytic performances exhibited by them.[19] In this work, we have used triblock copolymer P123-stabilized MoS_2 nanosheets as supporting materials for interfacing Cyt *c* and making a new nanobiocatalytic system with superior peroxidase-like catalytic activity. The MoS_2 nanosheets are of particular importance in this regard because: (1) they exhibit intrinsic peroxidase-like catalytic activity (therefore, they are often referred to as nanozymes) and (2) they can effectively interact with Cyt *c*, causing a conformational change to improve not only their own intrinsic catalytic activity but also the catalytic activity of Cyt *c*.[25] Therefore, the MoS_2-nanozyme-activated synergistic amplification of the catalytic activity of our

https://doi.org/10.1021/acsomega.2c00839
ACS Omega 2022, 7, 16593−16604

developed Cyt c−MoS_2 bionanohybrid catalyst is the major focus of the present work. Besides, we have also emphasized the understanding of the structural and conformational changes of the immobilized Cyt c on MoS_2 responsible for enhancing its catalytic efficiency. The peroxidase-like catalytic activity of the nanobiohybrid has been explored by probing the oxidation of a 2,2′-azino-bis-3-ethylbenzthiazoline-6-sulfonic acid (ABTS) substrate in the presence of another substrate H_2O_2.

2. EXPERIMENTAL SECTION

2.1. Materials. Molybdenum disulfide, pluronic P123 poly(ethylene oxide)-*b*-poly(propylene oxide)-*b*-poly(ethylene oxide) triblock copolymer ($PEO_{20}PPO_{70}PEO_{20}$), 2,2′-azino-bis-3-ethylbenzthiazoline-6-sulfonic acid (ABTS), and hydrogen peroxide (H_2O_2) were purchased from Sigma-Aldrich. Cytochrome c from horse heart and sodium phosphate monobasic (anhydrous) and sodium phosphate dibasic (anhydrous) used to prepare phosphate buffer (PB) solution were purchased from Sisco Research Laboratories (SRL), India. All the reagents were used as received without further purification.

2.2. Preparation of MoS_2 Nanosheets. MoS_2 nanosheets were prepared by an ultrasonication-assisted centrifugation method.[10,43,44] In a typical experiment, 11 mg/mL of MoS_2 solution was prepared in 1% (w/v) aqueous pluronic P123 polymer solution, and the solution was sonicated for 5 h in a 100 W bath sonicator. Then the dispersed solution was subjected to centrifugation at 7000 rpm (in RM-12 Micro Centrifuge) to remove the bigger particles, and the supernatant was taken out as MoS_2 nanosheet dispersion. Nanosheet dispersions were found to be stable over several weeks.

2.3. Preparation of Cyt c−MoS_2 Nanobiohybrids. The Cyt c−MoS_2 nanobiohybrid was prepared through the spontaneous adsorption of Cyt c on P123 polymer functionalized MoS_2 nanosheets. First, we prepared stock solutions of MoS_2 (21 μg/mL) and Cyt c (100 μM) in aqueous 10 mM, pH 7.1 phosphate buffer. Appropriate amounts of the MoS_2 and Cyt c from their respective stock solutions were mixed in phosphate buffer to obtain a series of Cyt c−MoS_2 nanobiohybrid-containing solutions with increasing concentration (from 0.5 μg/mL to 3 μg/mL) of MoS_2 and a fixed 0.5 μM concentration of Cyt c. These solutions were used to study the MoS_2 concentration-dependent catalytic activity of the nanobiohybrids. The solutions were stirred for 5 min at room temperature before performing catalytic studies. The nanobiohybrids with 3 μg/mL of MoS_2 and 0.5 μM Cyt c were used for kinetic analysis by studying catalytic activities under varying substrate (ABTS/H_2O_2) concentrations.

2.4. UV−vis Absorption, FTIR, and TEM Characterizations. UV−vis absorption studies of the MoS_2 nanosheets, Cyt c, and Cyt c−MoS_2 nanobiohybrids were performed using a spectrophotometer (model: LABINDIA-UV 3092).[44] The formation of the Cyt c−MoS_2 nanobiohybrid was confirmed by the observed shift of the Soret band position of Cyt c from 409 nm in the free native state to 400 nm in the bound state of the nanobiohybrids. The amount of Cyt c adsorbed on MoS_2 nanosheets was roughly estimated by spectrophotometric measurements of an aqueous buffer solution of Cyt c (10 μM) before and after addition of MoS_2 (10 μg/mL) into the solution. The decrease in absorbance of the free Cyt c at 409 nm (ε = 106 000 M^{-1} cm^{-1}) due to the adsorption has been used to roughly estimate the concentration of the adsorbed Cyt c.

For FTIR studies of the MoS_2 nanosheets and the Cyt c−MoS_2 nanobiohybrids, the suspensions were centrifuged at higher rpms (around 12 000 rpm) multiple times and collected the solid particles. The solid particles were washed three to four times with distilled water to remove weakly adsorbed polymer molecules and dried at 56 °C. The samples were analyzed with a Thermo Scientific-Nicolet iS5 FTIR spectrometer, in the frequency range of 500−4000 cm^{-1}.

TEM measurement of the MoS_2 nanosheets was carried out using a JEM−2100 HRTEM (Make−JEOL, Japan) instrument.[25]

2.5. Peroxidase Activity and Michaelis−Menten Kinetic Analysis. The peroxidase activity of immobilized Cyt c protein on MoS_2 was evaluated by measuring the initial rates of ABTS oxidation in the presence of H_2O_2. The formation of the oxidation product, the ABTS radical cation (ε_{418} = 3.6 × 10^4 M^{-1} cm^{-1}), was recorded by monitoring the time-dependent absorption increase at 418 nm. For the catalytic activity studies, a total 100 μL volume of the Cyt c−MoS_2 nanobiohybrid solution was taken in a cuvette (1 cm path length) and mixed with an appropriate concentration of ABTS (from a stock solution prepared in 10 mM phosphate buffer at pH 7.1). The absorption kinetics (at 418 nm) were started by the addition of H_2O_2. ABTS, H_2O_2, and nanobiohybrid samples were freshly prepared each time.

Peroxidase enzymatic kinetics of the Cyt c−MoS_2 nanobiohybrid (3 μg/mL of MoS_2 + 0.5 μM Cyt c) and MoS_2 (3 μg/mL) only systems as catalysts were analyzed using the Michaelis−Menten equation (eq 1), and the associated Lineweaver−Burk equation (eq 2) was used to obtain the kinetic parameters. In the Michaelis−Menten approach, the initial reaction rates (v_0) are measured at different initial substrate concentrations (S_0), and the kinetic parameters (V_{max}, k_{cat}, and K_m) are obtained from the linear fitting analysis of the Lineweaver−Burk plot (eq 2). In this work, the peroxidase-like catalytic cycle involves two substrates (H_2O_2 and ABTS). To obtain the Michaelis−Menten kinetic parameters with respect to both the substrates, the Lineweaver−Burk plots have been constructed from a series of experiments in which the concentration of one of the substrate is held constant while varying the other one. The kinetic parameters obtained from this treatment are only apparent constants.

$$v = k_{cat}E_0\frac{[S]}{K_m + [S]} \quad (1)$$

$$\frac{1}{v} = \left[\frac{K_m}{V_{max}}\right]\frac{1}{[S]} + \frac{1}{V_{max}} \quad (2)$$

Here "v" is the initial reaction rate; "$[S]$" is the substrate concentration; "$[E_0]$" is the total enzyme concentration; k_{cat} is the turnover rate constant; and K_m is the Michaelis−Menten constant.

2.6. Molecular Docking Analysis. Docking analysis was carried out to observe any probable molecular interactions between the protein Cyt c and the PEO units of the triblock copolymer that are attached to the MoS_2 nanosheet surface. A ligand, 2-[2-(2-hydroxyethoxy)propoxy]ethanol, was docked on a horse heart Cyt c molecule using "Autodock Vina" software. Grid box dimensions were set to be 40 Å for X, Y,

https://doi.org/10.1021/acsomega.2c00839
ACS Omega 2022, 7, 16593−16604

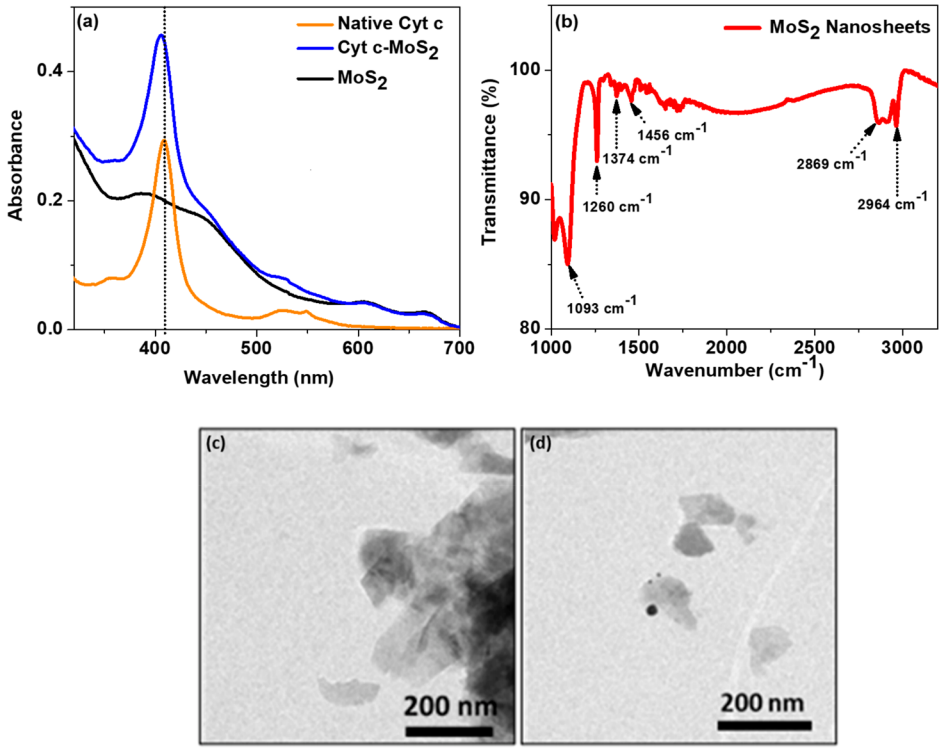

Figure 1. (a) Absorption spectra of MoS_2 nanosheets, native Cyt *c*, and the Cyt *c*−MoS_2 hybrid. (b) FTIR spectrum of P123 polymer stabilized MoS_2 nanosheets. (c, d) TEM images of the MoS_2 nanosheets.

and *Z* conformations. To analyze the nature of substrate−protein binding interactions, the Cyt *c* molecule was also docked with ABTS and H_2O_2 by the above procedure, in which the ligand was chosen as ABTS or H_2O_2.

3. RESULTS AND DISCUSSION

3.1. Spectroscopic and Microscopic Characterizations of MoS_2 Nanosheets. Figure 1a shows the absorption spectrum of MoS_2 nanosheet dispersion in aqueous P123 solution. The spectral characteristics share common features of the trigonal prismatic-coordinated 2H phase of MoS_2.[45] The two characteristic absorption bands in the 600−700 nm region of the spectrum correspond to the excitonic transition of MoS_2 from the valence bands to the minima of the conductance band (at the K point of the Brillouin zone). The splitting of the valence band by spin−orbit and interlayer coupling interactions accounts for the two excitonic bands.[9,46] There are two additional higher energy absorption bands in the 350−450 nm region of the spectra corresponding to the transition of electrons to the higher density states of the Brillouin zone.[47] The concentration of the as-prepared MoS_2 nanosheet dispersion was calculated using the absorbance value at 345 nm, for which the extinction coefficient was previously reported as 6820 L g^{-1} cm^{-1}.[44] The concentration of the prepared nanosheet solution was found to be 21 μg/mL.

The FTIR spectrum of the P123 triblock copolymer coated MoS_2 nanosheets is given in Figure 1b. The corresponding spectra of the bulk MoS_2 material and the P123 polymer are given in Figure S1 of the Supporting Information. The FTIR results confirm that the surface of the MoS_2 nanosheets is functionalized with the P123 polymers. The presence of CH_3 groups of the central hydrophobic PPO blocks of the polymer on the MoS_2 nanosheets is confirmed by the two bands at ∼2965 and ∼1374 cm^{-1}. The 2965 cm^{-1} band can be assigned to the antisymmetric C−H stretching vibration of the methyl groups and the 1374 cm^{-1} band to the symmetric deformation band of the methyl groups. The FTIR peak at 2869 cm^{-1} corresponds to the antisymmetric methylene (CH_2) stretching modes. The 1093 cm^{-1} band is due to the C−O−C stretching vibration of the P123 polymer. These characteristic FTIR bands of the P123 polymer on the MoS_2 nanosheets are consistent with the FTIR spectrum of the pure P123 polymer (Figure S1).[48] The other bands peaking at 1627 and 1260 cm^{-1} correlate well with the FTIR absorption bands of MoS_2.[49]

The TEM images of the P123 polymer stabilized MoS_2 nanosheets are given in Figure 1c,d. These images confirm the two-dimensional nanosheet structure of the synthesized MoS_2. Moreover, the average dimension of the exfoliated individual nanosheets is found in the range of 90−100 nm.

3.2. Length and Thickness of the MoS_2 Nanosheets. The mean length and thickness of the MoS_2 nanosheets can be calculated using previously reported empirical relations based on the information at the characteristic A (at 660 nm) and B (at 610 nm) excitonic bands of the prepared MoS_2 nanosheets. The length of the MoS_2 nanosheet is related to the ratio of the extinction coefficient at the B-excitonic peak (E_B) to that at 345 nm (E_{345}) by the following relation:[44]

$$L\ (\mu\text{m}) = \frac{3.5\frac{E_B}{E_{345}} - 0.14}{11.5 - \frac{E_B}{E_{345}}} \quad (3)$$

The thickness of the nanosheets (referred to as number of MoS_2 layers in each nanosheet, N_{MoS_2}) can be obtained from the peak position of the A-exciton band using the following relation:[44]

$$N_{MoS_2} = 2.3 \times 10^{36} e^{-54888/\lambda_A} \quad (4)$$

https://doi.org/10.1021/acsomega.2c00839
ACS Omega 2022, 7, 16593−16604

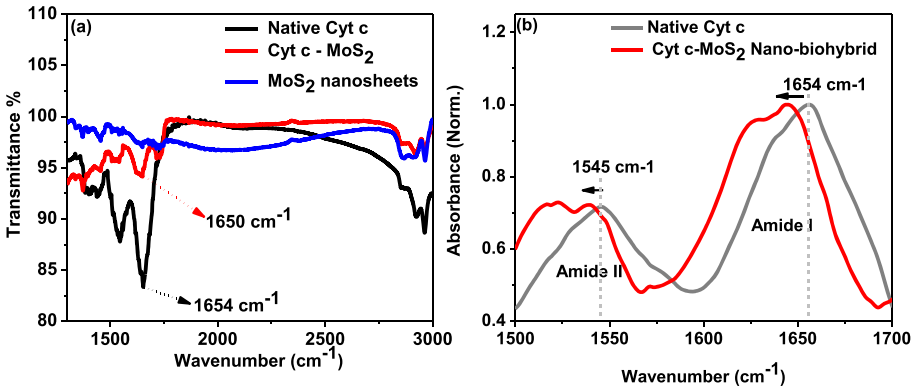

Figure 2. (a) FTIR spectra of native Cyt *c*, the Cyt *c*−MoS_2 nanobiohybrid, and free MoS_2 nanosheets. (b) FTIR spectra of free and bound Cyt *c* focusing on the amide I and amide II regions.

Using the above relations, the calculated length and thickness of the MoS_2 nanosheets are found to be ∼90 nm and ∼3.4 layers/nanosheet, respectively. The calculated length of the MoS_2 nanosheets is found to be well correlated with the average dimension obtained from TEM results.

3.3. Characterization of the Cyt *c*−MoS_2 Nanobiohybrid System. The P123 stabilized MoS_2 nanosheets were used for the formation of a Cyt *c*−MoS_2 hybrid nanobiocatalytic system through the adsorption of Cyt *c* on the MoS_2 nanosheets. The formation of an interactive bionanointerface can be understood from UV−visible absorption spectral changes of Cyt *c* before and after adsorption on MoS_2. Cyt *c* in its native oxidized state shows a highly intense Soret band at 409 nm and two other relatively low intense peaks around 522 and 360 nm named as Q and δ band, respectively (Figure 1a). The two visible region bands (Q and Soret bands) originate from the π to π^* transitions of the porphyrin ring.[50] The Soret band is highly sensitive to the heme microenvironment of Cyt *c*. Any perturbations in and around heme will be reflected by the change in the peak position and/or intensity of the Soret band.[42] After being stirred with MoS_2 nanosheets, the Cyt *c* native Soret band position at 409 nm has been found to be blue-shifted to 400 nm. This clearly indicates possible interactions between Cyt *c* and the MoS_2 nanosheet template that might lead to some perturbations on the heme center suitable for peroxidase activity enhancement. Based on the decreased absorbance of the free native Cyt *c* at 409 nm upon adsorption on MoS_2, the amount of adsorbed Cyt *c* on the MoS_2 nanosheets was estimated as 1.12 μM in 10 μg/mL of MoS_2 solution.

The influence of MoS_2 nanosheets on Cyt *c* is further supported by the FTIR analysis. The FTIR spectra of native Cyt *c*, the Cyt *c*−MoS_2 nanobiohybrid, and free MoS_2 nanosheets are given in Figure 2. The major characteristic amide I peak of the protein that arises from the carbonyl functionality of the peptide linkage has been shifted from 1654 cm^{-1} in the native state to 1650 cm^{-1} in the nanobiohybrid state. A similar shift (from 1545 cm^{-1} in the native state to 1541 cm^{-1} in the hybrid state) is also observed for the amide II region of the protein in the FTIR spectra (Figure 2b). Based on the correlation between the amide I band positions and the secondary structure of the proteins, the 1654 cm^{-1} band can be attributed to the α-helices, and the bands in the lower- and higher-frequency regions at 1629 and 1675 cm^{-1} correspond to the vibrations in β-sheet structure. Any major changes (position and intensity) of the amide I and II absorption bands are considered to be associated with the protein's secondary structural variations.[50]

Ye et al. previously reported a similar FTIR spectral shift (from 1653 to 1649 cm^{-1}) with a concomitant decrease in intensity of the amide I band of Cyt *c* upon increasing temperature.[51] This was assigned to the partial unfolding of the protein segment containing Met-80 which led to the disruption of the S−Fe bond at the heme coordination site. A similar structural perturbation can be expected for the Cyt *c* upon binding with MoS_2. Such minor structural changes at the heme center are suitable for the activation of the peroxidase-like behavior of Cyt *c*. However, a major structural deviation or a complete unfolding would conversely affect protein's catalytic activity.

3.4. Molecular Docking Analysis. The PEO and PPO units of P123 polymer coated on the surface of MoS_2 nanosheets can interact and help in assembling a greater number of Cyt *c* on the nanosheets. To understand the possible interactions between Cyt *c* and the PEO and PPO units of P123 on the MoS_2 surface, molecular docking analysis was performed using 2-[2-(2-hydroxyethoxy)propoxy]ethanol [$OH(CH_2CH_2O)(CH(CH_3)CH_2O)CH_2CH_2OH$] as a ligand. A binding energy of −3.7 kcal mol^{-1} was obtained for the best docking conformation of the protein with the ligand. The hydroxy-ethoxy moiety mainly exhibits polar hydrogen bonding interactions with the neighboring amino acids of the protein, such as arginine 38, glycine 23, histidine 33, glycine 34, and asparagine 31, either directly or through water molecules (Figure S2). Some nonpolar interactions can be observed from a central propoxy moiety which is relatively hydrophobic in nature. Parray et al.[45] have recently indicated that the interaction of Cyt *c* with polyethylene glycol (with an interaction energy of −3.9 kcal mol^{-1}) does not significantly perturb the Met 80-heme structure of Cyt *c*, meaning that the protein binds to PEG without major structural deviations. In the P123-supported MoS_2 system, the PEO (PEG) units provide a soft template for protein binding interactions and help to prevent major structural changes of Cyt *c*.

3.5. Enhanced Peroxidase Activity of the Cyt *c*−MoS_2 Nanobiocatalyst. The peroxidase-like activity of the Cyt *c*−MoS_2 nanobiocatalyst has been explored with the catalytic oxidation of ABTS (the chromogenic substrate) in the presence of H_2O_2. The appearance of an intense green color of the solution resulting from the generation of the ABTS radical cation (oxidized form of ABTS) provides initial evidence for the peroxidase activity of the nanobiohybrid

https://doi.org/10.1021/acsomega.2c00839
ACS Omega 2022, 7, 16593−16604

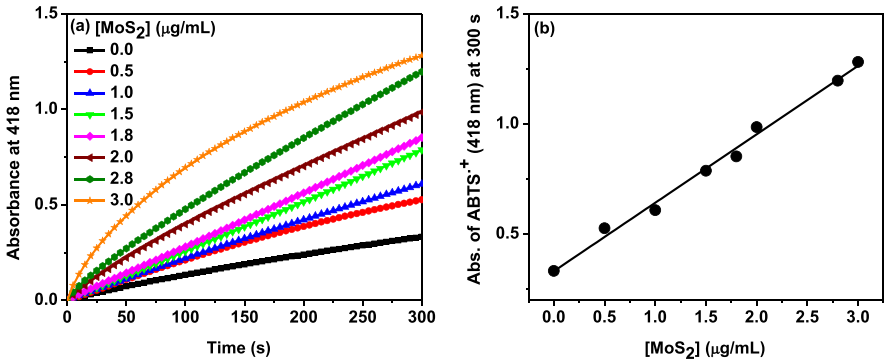

Figure 3. (a) Increase of peroxidase activity of Cyt *c* (0.5 μM) in the presence of increasing concentration of MoS_2 (0−3 μg/mL) as shown by the time-dependent absorbance increase of the ABTS radical (oxidized form of ABTS) at 418 nm. The concentration of ABTS = 0.5 mM and H_2O_2 concentration = 5 mM. (b) Plot of the absorbance value of the oxidized product of ABTS formed at 300 s vs concentration of MoS_2, showing the linear relationship between them.

system. To understand the role of interactions between Cyt *c* and MoS_2 in modulating the catalytic activity of the hybrid system, we have also performed the catalytic oxidation of ABTS using free Cyt *c* and the MoS_2 nanosheets separately. The quantitative analysis of the catalysis was obtained from the time-dependent absorbance changes of the solutions at 418 nm, which is the characteristic absorption wavelength maximum of the ABTS radical cation formed during the reaction. The increase in absorbance (at 418 nm) with increasing time corresponds to an increase in concentration of the ABTS radical and thus provides kinetic information about the catalysis.

Figure 3a shows the absorption kinetic curves recorded immediately after addition of 5 mM H_2O_2 to a series of reaction solutions containing fixed concentrations of ABTS (0.5 mM) and Cyt *c* (0.5 μM) with an increasing concentration (0−3.0 μg/mL) of MoS_2 nanosheets in 10 mM phosphate buffer of pH 7.1. Before H_2O_2 addition, the solutions were stirred and equilibrated for 5 min to ensure sufficient adsorption of Cyt *c* on MoS_2 nanosheets for effective catalysis reaction. The background absorptions of the reaction solutions before H_2O_2 addition were subtracted to get the actual concentration of the ABTS radical cation formed at any given time of the reaction by converting the absorbance values into concentration using an extinction coefficient of 3.6×10^4 M^{-1} cm^{-1} of the radical cation at 418 nm.[39,52]

In the absence of MoS_2, free Cyt *c* resulted in only a slight increase in absorbance at 418 nm (over 300 s reaction time), suggesting weak peroxidase activity of free Cyt *c* in solution (Figure 3a). This is consistent with previous reports.[41] The peroxidase activity of the free Cyt *c* remains unchanged in the presence of 1% (w/v) P123 polymer, which has been used to stabilize the MoS_2 nanosheets (Figure S3a). However, the presence of P123 polymer coated MoS_2 nanosheets as a supporting system significantly enhances the extent of absorbance increase (over the same reaction time) with a faster kinetics of ABTS radical cation formation. As the concentration of MoS_2 nanosheets increases from 0 to 3 μg/mL, the absorbance at 418 nm at 300 s reaction time is increased linearly without leveling off (Figure 3b).

It is noteworthy to mention that, like graphene oxide,[53] MoS_2 nanosheets are also intrinsically active toward peroxidase catalysis, and the activity is highly dependent on the nature of surface modifications, as recently reported by Yu et al.[25] Therefore, we have studied the catalytic activity of our synthesized MoS_2 nanosheets alone at different concentrations (1 to 3 μg/mL) without Cyt *c* as control experiments (Figure S3b). A lower extent of absorbance increase of the ABTS radical cation was observed for the MoS_2 nanosheets alone as catalysts compared to that observed for the nanobiohybrid catalyst containing the same concentration of MoS_2 with 0.5 μM Cyt *c* (Figures 3 and S3b). The Cyt *c*−MoS_2 nanobiohybrid system containing 3 μg/mL of MoS_2 with 0.5 μM of Cyt *c* provided a yield of 36 μM ABTS radical cation at 5 min of reaction time, while the same concentrations of the free Cyt *c* (without MoS_2) and MoS_2 nanosheets (without Cyt *c*) separately yielded 9 μM and 22 μM of the ABTS radical. Thus, a clear and profound enhancement of catalytic activity is observed for the Cyt *c*−MoS_2 nanobiocatalyst compared to the free MoS_2 nanosheets and native Cyt *c*, highlighting the importance of nanobiointerfaces for effective catalysis reactions.

Weak peroxidase activity of native Cyt *c* can be attributed to the lower accessibility of the substrate to the six-coordinated structure with a low spin heme center protected by its native protein environment.[40,54] This is in contrast to that of a true peroxidase where a five-coordinated heme center with an almost vacant or loosely bound sixth coordination site allows easy access to the substrate to initiate peroxidase activity.[37] The enhanced peroxidase-like catalytic activity of Cyt *c* on MoS_2 can be due to the structure−function switching of Cyt *c* from its typical redox protein state into a well-performing peroxidase mimic. The interaction of Cyt *c* with the MoS_2 nanosheets probably led to partial unfolding of Cyt *c* with the slight perturbation of the heme structure, making the active site accessible to the substrates. The structural perturbation of the heme environment of Cyt *c* upon interactions with the MoS_2 nanosheets has already been confirmed from the UV−visible and FTIR analysis.

The MoS_2 nanosheets are known to have surface negative charge. Quinn et al.[43] previously reported a low negative surface charge (an approximate zeta potential of −13 mV) of the pluronic triblock copolymer supported MoS_2 nanosheets at pH 6.5. Based on this, the initial adsorption of the positively charged protein Cyt *c* on MoS_2 can be influenced by electrostatic attraction forces. However, as the MoS_2 nanosheet surface is covered with nonionic polymer P123, the hydrogen bonding and hydrophobic interactions between the polymer units (PEO and PPO moieties) and Cyt *c* will also play

https://doi.org/10.1021/acsomega.2c00839
ACS Omega 2022, 7, 16593−16604

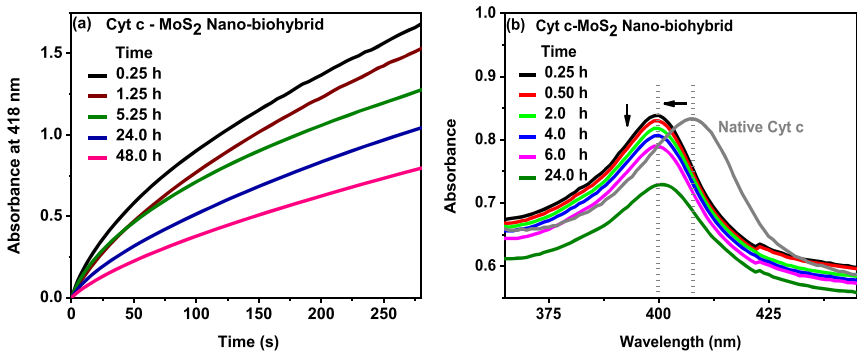

Figure 4. (a) Time-dependent peroxidase activity changes of the Cyt *c*−MoS_2 nanobiohybrid. The peroxidase activity of the Cyt *c*−MoS_2 nanobiohybrid was measured at different time periods of incubation of Cyt *c* (0.5 μM) with MoS_2 (3 μg/mL). Catalytic activity was studied with 0.5 mM ABTS and 5 mM H_2O_2. (b) Time-dependent UV−vis absorption spectral change of Cyt *c* during the interaction with MoS_2 nanosheets.

important roles in anchoring the Cyt *c* on the MoS_2 nanosheets for enhanced catalytic activity of the hybrid.

The influence of electrostatic forces on the peroxidase catalytic activity of the nanobiohybrid system was studied with the addition of 1 M NaCl into the reaction mixture (Figure S4a). The catalytic activity of the nanobiohybrid catalyst is found to be only slightly decreased in the presence of 1 M NaCl. For a better understanding, we have plotted the catalytic rate vs time curves in the absence and presence of 1 M NaCl as given in Figure S4b. From this figure, we can see that the decrease in catalytic activity is more pronounced at the initial reaction time (0−50 s), suggesting the influence of electrostatic forces at the initial stage of the reaction. At longer reaction time (50−300 s), the reactions in the absence and presence of NaCl converges to a state where the catalytic reaction progresses at a similar reaction velocity of 0.05 μM s^{-1}. Therefore, it can be inferred that increasing ionic strength reduces the initial activity through electrostatic forces, thereby leading to slightly lower concentration of the $ABTS^{\bullet+}$ formed at any equal time points. A strong influence of electrostatic forces on the catalytic activity was earlier reported for Cyt *c* on graphene oxide because of the presence of various ionizable polar groups on graphene oxide.[39,40]

The effect of pH on the catalytic activity of the Cyt *c*−MoS_2 nanobiocatalyst was studied by preparing the reaction mixtures in phosphate buffers of pH 3.7, 7.1, and 10.3 (Figure S5a). The catalytic activity of the Cyt *c*−MoS_2 nanobiohybrid significantly increases with decreasing pH of the medium. A similar trend is also observed for the control experiments using Cyt *c* (without MoS_2) and MoS_2 (without Cyt *c*) as catalysts (Figure S5b,c). Acidic pH enhances the peroxidase activity, whereas the basic pH significantly reduces the activity. However, in any particular pH condition, the catalytic activity of the Cyt *c*−MoS_2 nanobiohybrid is significantly higher than the activity of the individual components, MoS_2 and Cyt *c* (Figure S5). The acidic pH condition facilitates the approach of the negatively charged substrate ABTS to the MoS_2 nanosheets and thereby improves the catalytic activity. Moreover, in the case of the nanobiohybrid, the acidic pH conditions probably provide more favorable conditions for the adsorption of Cyt *c* on the MoS_2 surface.[39] Both MoS_2 and Cyt *c* separately exhibit negligible catalytic properties in basic pH, while a weak activity is observed for their nanobiohybrid. The observed pH dependence is consistent with the previous reports on the peroxidase-like activity using a wide variety of catalytic systems. Gao et al.[55] earlier reported an optimal pH of 3.5 for the intrinsic peroxidase-like activity of Fe_3O_4 nanoparticles. The activity of a peroxidase enzyme HRP was also shown to be optimum in similar acidic regions.

3.6. Time-Dependent Study of Catalytic Activity. Time-dependent variations in the catalytic activity of Cyt *c*−MoS_2 nanobiohybrids were studied by monitoring the H_2O_2-mediated ABTS oxidation kinetics at different incubation times of Cyt *c* with MoS_2. For this, a solution containing the nanobiohybrids was prepared by mixing 0.5 μM Cyt *c* and 3 μg/mL of MoS_2 in aqueous buffer solution and its catalytic activity was assessed at different incubation times up to 48 h after mixing. With increasing incubation time, the catalytic activity of the nanobiohybrid was found to be decreased (Figure 4a). This is evidenced by the slower kinetics of ABTS oxidation with a lower extent of absorbance increase observed at a longer incubation period compared to that observed at a shorter incubation period. The reduced catalytic activity of the Cyt *c*−MoS_2 hybrid at longer incubation time is also supported by the time-dependent decrease in intensity of the Soret band of Cyt *c* upon adsorption on MoS_2 (Figure 4b). Immediately after mixing Cyt *c* with MoS_2 (within 10−15 min), the generation of the Cyt *c*−MoS_2 bionanointerface has caused a blue shift of the Soret band from 409 nm (characteristic of the native Cyt *c*) to 400 nm. As a result, the Cyt *c* gets activated for effective peroxidase like behavior. As the incubation time progresses, the intensity of the resultant 400 nm absorption band is gradually reduced, consistent with the observed loss of peroxidase activity (Figure 4). At 24 h of incubation, the absorbance of Cyt *c* is significantly reduced, and consequently the catalytic activity is dramatically decreased. This can be due to the degradation of the protein after a long incubation period (24 and 48 h).

3.7. Michaelis−Menten Kinetic Analysis. The catalytic activity of the Cyt *c*−MoS_2 bionanohybrid catalyst presented in this work can be viewed as a bisubstrate-based peroxidase-like catalysis reaction. The ABTS substrate is oxidized in the presence of another substrate H_2O_2, producing the ABTS radical cation ($ABTS^{\bullet+}$) as the product. Previously, multiple irreversible reaction steps were used to describe the peroxidase catalysis as shown in Scheme 2.[56] The first step of the peroxidase cycle involves a rapid two-electron oxidation of the catalyst by H_2O_2, producing an intermediate Compound I.

Compound I is converted back to the catalyst by two successive electron transfer reactions from the ABTS substrate (Scheme 2). The first step is reported to be highly rapid, and therefore, the rate of product formation is largely dependent

https://doi.org/10.1021/acsomega.2c00839
ACS Omega 2022, 7, 16593−16604

Scheme 2. Schematic Representation of the Peroxidase Catalytic Cycle Involving Multiple Irreversible Steps

$$\text{Catalyst} + H_2O_2 \xrightarrow{k_a} \text{Compound I} + H_2O$$

$$\text{Compound I} + \text{ABTS} \xrightarrow{k_b} \text{Compound II} + \text{ABTS}^{\cdot+}$$

$$\text{Compound II} + \text{ABTS} \xrightarrow{k_c} \text{Catalyst} + \text{ABTS}^{\cdot+} + H_2O$$

on the reducing substrate ABTS.[56] In the case of horseradish peroxidase isoenzyme C, the rate constants follow the order $k_a > k_b \gg k_c$.[57] In the above model, the kinetic steps are considered as irreversible, assuming a linear kinetics of product formation. However, a large number of recent reports have suggested the reversible nature of the binding of H_2O_2 to the enzyme before forming the intermediate compound I, justifying the applicability of the Michaelis–Menten kinetic model with evidence of saturated kinetics in peroxidase-like catalytic activities.[25,32,38,39,41]

Here we have analyzed the kinetic data for the peroxidase activity of the Cyt *c*–MoS_2 nanobiohybrid catalyst with ABTS–H_2O_2 as a dual substrate system using the Michaelis–Menten theory by applying eqs 1 and 2. To obtain the kinetic parameters using this model, the steady-state reaction kinetics were monitored by varying substrate concentration. The ABTS concentration variation (from 0.2 to 1 mM) kinetics assay was performed by keeping the H_2O_2 fixed at an excess concentration of 5 mM (Figure 5a). Similarly, for the kinetics assay measurements with varying H_2O_2 concentration (from 2 to 10 mM), the ABTS concentration was kept fixed at 0.5 mM (Figure S6a). The absorbance kinetics were converted into the time-dependent concentration changes of the ABTS radical cation by using the molar extinction coefficient of the ABTS radical cation ($\varepsilon_{418} = 3.6 \times 10^4$ M^{-1} cm^{-1}). The apparent steady-state reaction rates at the initial stage of the reaction at different substrate concentrations were obtained from the initial slope of the concentration kinetic curves. The initial reaction rates (v) vs substrate concentration plots were found to be hyperbolic (Figures 5b and S6b).

The Lineweaver–Burk plots (Figure 6) exhibit linear characteristics, suggesting that the catalytic behavior of the Cyt *c*–MoS_2 nanobiohybrid follows the Michaelis–Menten enzymatic kinetics for both the ABTS and H_2O_2 as substrates. The fitting analysis of the Lineweaver–Burk plots is provided by the Michaelis–Menten kinetic parameters, as given in Table 1. The Michaelis–Menten constant (K_m) is inversely related to the catalyst–substrate binding affinity. A lower K_m value is desirable for a newly designed catalyst to obtain higher catalytic efficiency (k_{cat}/K_m).[39] The K_m values of the Cyt *c*–MoS_2 nanobiohybrid catalyst are found to be 1.20 and 2.94 mM for the ABTS and H_2O_2 substrates, respectively. Similar low K_m values were earlier reported for the peroxidase activity of Cyt *c* using graphene oxide, silica nanoparticles, and polymer scaffold as supporting systems.[32,38,39] The K_m value of the Cyt *c*–MoS_2 nanobiohybrid is significantly lower than that of the free Cyt *c* (123 mM).[41] This suggests that Cyt *c* has a higher substrate binding affinity when adsorbed on the MoS_2 nanosheets.

Consistent with the literature reports, a lower K_m value is observed for the nanobiocatalyst against the ABTS substrate compared to the H_2O_2 substrate, indicating more profound catalyst–ABTS binding affinity than catalyst–H_2O_2 binding.[39] This is primarily due to the electrostatic interactions between the negatively charged ABTS substrate and the positively charged Cyt *c* that are adsorbed on the surface of the P123 coated MoS_2 nanosheets at a physiological pH. This observation is further supported by the docking analysis for native Cyt *c* against ABTS as well as H_2O_2. A binding energy of −2.8 kcal mol^{-1} was observed with Cyt *c*–H_2O_2 docking. While a much more negative binding energy of −6.1 kcal mol^{-1} was obtained for the Cyt *c*–ABTS docking pair (Figure S7), ABTS primarily interacted with the protein surface and the H_2O_2 docks near to the central heme unit.

The catalytic efficiency (k_{cat}/K_m) values of the Cyt *c*–MoS_2 nanobiohybrid catalyst are found to be 1633 and 265 M^{-1} s^{-1} for the ABTS and H_2O_2 substrates, respectively. The higher (k_{cat}/K_m) value of the catalyst for the ABTS substrate compared to the H_2O_2 substrate is consistent with the higher affinity of Cyt *c* toward the ABTS substrate. Moreover, the (k_{cat}/K_m) value of the Cyt *c*–MoS_2 hybrid catalyst is also found to be significantly higher than that of the previously reported value for free Cyt *c* (8 M^{-1} s^{-1}),[41] suggesting better catalytic performance of Cyt *c* upon adsorption on MoS_2 nanosheets.

We further examined the Michaelis–Menten kinetics of the MoS_2 nanosheets (3 μg/mL) without Cyt *c*. To obtain the kinetic parameters, the substrate (ABTS/H_2O_2) concentration dependent steady-state absorption kinetic assays for the MoS_2 nanosheets alone as catalysts were performed. For the ABTS substrate concentration variation assay, the concentration of ABTS was varied in the range 0.06–0.50 mM, keeping H_2O_2

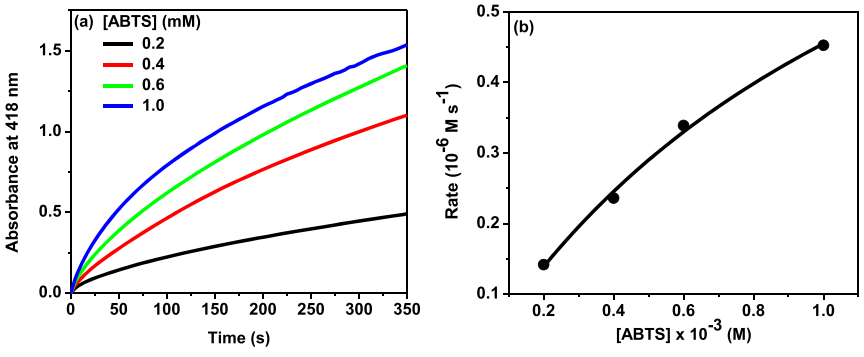

Figure 5. (a) Steady-state kinetic assay of the Cyt *c*–MoS_2 nanobiohybrid (0.5 μM Cyt *c* + 3 μg/mL of MoS_2) with varying concentrations of ABTS substrate as shown by monitoring the time-dependent absorbance changes of the ABTS radical (oxidized form) at 418 nm. The concentration of H_2O_2 was kept constant at 5 mM in each kinetic assay. (b) Initial peroxidase reaction rates (v) for the Cyt *c*–MoS_2 nanobiohybrid with increasing concentration of ABTS.

https://doi.org/10.1021/acsomega.2c00839
ACS Omega 2022, 7, 16593–16604

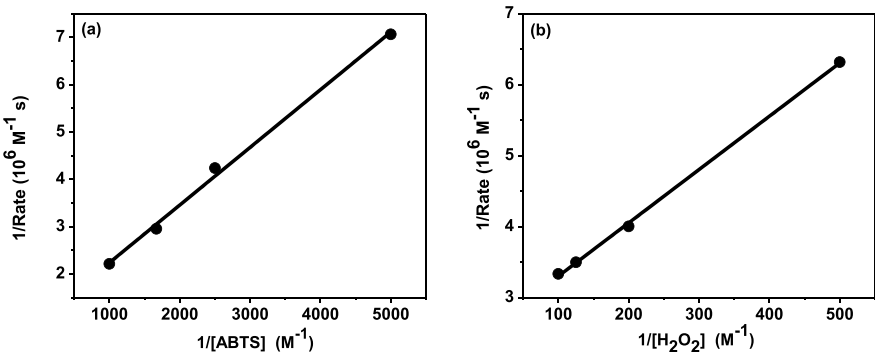

Figure 6. Double reciprocal plots of the kinetic assays of the Cyt *c*−MoS_2 nanobiohybrid system (a) at varying concentration of the ABTS substrate while keeping the H_2O_2 concentration fixed at 5 mM and (b) at varying concentration of H_2O_2 while keeping the ABTS concentration fixed at 0.5 mM. These plots were used to calculate the catalytic Michaelis−Menten parameters.

Table 1. Michaelis−Menten Kinetic Parameters for Cyt *c*−MoS_2 Nanobiohybrids and MoS_2 Nanosheets As Catalysts with Respect to ABTS and H_2O_2 Substrates

catalytic system	substrate	k_{cat} (s^{-1})	K_m (mM)	k_{cat}/K_m (M^{-1} s^{-1})
Cyt *c*−MoS_2 nanobiohybrid catalyst	ABTS	1.96	1.20	1633
	H_2O_2	0.78	2.94	265
MoS_2	ABTS	0.035	0.32	109
	H_2O_2	0.017	0.16	106

concentration fixed at 5 mM (Figure S8). On the other hand, the H_2O_2 concentration variation kinetic assay was obtained in the range 0.02−2 mM, keeping the ABTS concentration fixed at 0.5 mM (Figure S9). The MoS_2 nanosheets (3 μg/mL) without Cyt *c* exhibit Michaelis−Menten kinetic behavior for both the substrates. This is evidenced from the hyperbolic plots of the initial rate vs substrate concentration as given in Figures S8b and S9b. The kinetic parameters obtained from the linear Lineweaver−Burk plots (Figure S10) are given in Table 1. The catalytic efficiency (k_{cat}/K_m) values of the P123 stabilized MoS_2 nanosheets alone are found to be around 109 and 106 for the ABTS and H_2O_2 substrates, respectively. The catalytic efficiency of the MoS_2 nanosheets alone is significantly weaker than the corresponding Cyt *c*−MoS_2 nanobiohybrid. Therefore, free MoS_2 nanosheets alone only weakly contribute to the enhanced peroxidase activity of the Cyt *c*−MoS_2 nanobiohybrid.

3.8. Reaction Progress Kinetic Analysis. The peroxidase-like catalytic cycle involves two substrates (H_2O_2 and ABTS) with multiple reaction steps. The kinetic analysis of such multistep- and multisubstrate-based catalytic reactions is complicated. The Michaelis−Menten kinetic model has been extensively applied to describe peroxidase-like catalytic activity for a wide variety of catalysts. However, it is important to note that the kinetic parameters (V_{max} and K_m) obtained from this analysis for varying initial concentrations of a particular substrate will be dependent on the concentration of the other substrate. Thus, the obtained Michaelis−Menten kinetic parameters are considered to be only apparent constants. This can be better understood if we consider a simple possible mechanism for a bisubstrate-based catalytic cycle, as given in Scheme 3.

The rate of the reaction as derived under pseudo-steady-state conditions is given by (eq 5):

Scheme 3. Mechanism for Bisubstrate-Based Simple Catalytic Cycles Involving Two Steps

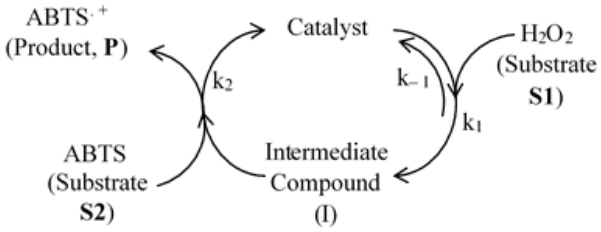

$$\text{Rate } (v) = \frac{\frac{k_1}{k_{-1}} k_2 [\text{Cat}]_{\text{total}} [\text{H}_2\text{O}_2][\text{ABTS}]}{1 + \frac{k_1}{k_{-1}}[\text{H}_2\text{O}_2] + \frac{k_2}{k_{-1}}[\text{ABTS}]} \quad (5)$$

The rate equation can be written in the form of the Michaelis−Menten type equation for the varying concentrations of ABTS substrate (eq 6) as

$$v = \frac{v^*_{max}[\text{ABTS}]}{K^*_m + [\text{ABTS}]} \quad (6)$$

where $v^*_{max} = k_1[\text{Cat}]_{\text{total}}[\text{H}_2\text{O}_2]$ and $K^*_m = \left(\frac{\frac{k_{-1}}{k_1} + [\text{H}_2\text{O}_2]}{\frac{k_2}{k_1}}\right)$

From this equation it is clear that both the K^*_m and v^*_{max} values are dependent on the concentration of $[\text{H}_2\text{O}_2]$. However, if the H_2O_2 concentration is taken in large excess so that its concentration can be assumed to be constant during the reaction, the kinetic parameters with respect to the ABTS substrate can easily be obtained from the Lineweaver−Burk plot.

Under the conditions of varying concentrations of both the substrates during the reaction, the reaction−progress−kinetic (RPK) analysis[58] provides an important understanding about the reaction mechanism and the orders of the reaction. In this graphical method, one needs to plot reaction rate vs substrate concentration by combining the substrate concentration vs time and the reaction rate vs time plots. In our peroxidase-like catalysis experiment, we record the accumulation of the product ($ABTS^{\bullet+}$) concentration (in terms of its absorbance) with increasing time. The rate vs time data were obtained by differentiating the product concentration vs time data. On the other hand, the substrate concentration vs time data were created by subtracting the product concentration vs time data

https://doi.org/10.1021/acsomega.2c00839
ACS Omega 2022, 7, 16593−16604

from the initial substrate concentration used in the reaction. By combining the rate vs time data and substrate concentration vs time data, we obtained the rate vs substrate concentration plot (Figure S11) for the catalytic system with 1 mM ABTS, 5 mM H_2O_2, and 0.5 μM Cyt *c* supported on 3 μg/mL of MoS_2 as a catalyst. It is important to note that this plot describes the rate of the catalytic reaction as the ABTS substrate is consumed from right to left because the substrate concentration decreases from the initial concentration as the product forms over the course of the reaction. The plot shows a curved feature, indicating a complex relationship between the rate and the substrate ABTS as described in the rate equation (eq 5).

We have applied variable-time-normalization analysis (VTNA) following a reported procedure to find the order of the reaction with respect to the hybrid catalyst.[59] In this analysis, the time scale of the two reactions run with different catalyst loadings is substituted by the normalized time scale, $\sum[C]^{\gamma}\Delta t$ (eq 7).

$$\sum [C]^{\gamma}\Delta t = \sum_{i=1}^{n} \left(\frac{[C]_i + [C]_{i-1}}{2}\right)^{\gamma} (t_i - t_{i-1}) \quad (7)$$

where $[C]$ is the concentration of the catalyst, and the value of "γ" that produces the overlay of the curves is the order in catalyst. The normalization term is based on the fact that the concentration of the catalyst is constant during the entire reaction without any deactivation. We have used this "constant normalization" of the time scale method to overlay the curves of two different kinetic profiles recorded using two different concentrations of the catalyst (3 and 2 μg/mL of MoS_2 with a fixed 0.5 μM of Cyt *c*). The overlay analysis of the curves in this concentration range of the MoS_2 gave the order of the reaction with respect to the catalyst as 2 (Figure S12).

4. CONCLUSION

In conclusion, a new nanobiocatalytic system has been prepared through the spontaneous adsorption of Cyt *c* on a triblock copolymer, P123, stabilized MoS_2 nanosheet. The catalytic activity of these nanobiohybrid systems has been successfully demonstrated by studying H_2O_2-mediated oxidation of the ABTS substrate. The enhanced catalytic performance of the Cyt *c*−MoS_2 nanobiohybrid catalyst compared to that of the free Cyt *c* and MoS_2 nanosheets can be explained based on the minor structural perturbation of the active site of the Cyt *c* upon adsorption on MoS_2 nanosheets. The triblock copolymer support on the MoS_2 nanosheets plays an important role in protecting the proteins from undergoing major structural changes. Moreover, the polymer support attracts more proteins to be adsorbed on the MoS_2 nanosheets and thereby increases the catalytic performance. From the study of Michaelis−Menten kinetics analysis, it is revealed that the adsorption of Cyt *c* on P123 stabilized MoS_2 nanosheets significantly increases the substrate binding affinity as well as the catalytic efficiency. Such a nanobiocatalytic system exhibiting high stability with enhanced catalytic activity may find their potential applications in biosensing, biofuel cells, and biomedical fields.

■ ASSOCIATED CONTENT

Supporting Information

The Supporting Information is available free of charge at https://pubs.acs.org/doi/10.1021/acsomega.2c00839.

FTIR spectra of bulk MoS_2 and P123 polymer; molecular docking analysis; peroxidase-like catalytic activity of native Cyt *c* (without MoS_2 nanosheets) and MoS_2 nanosheets (without Cyt c); ionic strength dependence of peroxidase-like activity of the Cyt *c*−MoS_2 nanobiohybrid; effect of pH on peroxidase-like activity of the Cyt *c*−MoS_2 nanobiohybrid and Cyt *c*-only, and MoS_2-only systems; steady-state kinetic assay and initial rates versus substrate concentration plots of Cyt *c*−MoS_2 nanobiohybrid and MoS_2-only systems; plot of rate vs ABTS substrate consumption as obtained from reaction progress kinetic analysis; and variable-time-normalization analysis for the determination of the order in catalyst (PDF)

■ AUTHOR INFORMATION

Corresponding Author

Sarthak Mandal − *Department of Chemistry, National Institute of Technology, Tiruchirappalli, Tamil Nadu 620015, India;* orcid.org/0000-0002-5592-9664; Email: smandal@nitt.edu, sarthakmandal@gmail.com

Authors

Anu Maria Chittilappilly Devassy − *Department of Chemistry, National Institute of Technology, Tiruchirappalli, Tamil Nadu 620015, India*

Adithya Kamalakshan − *Department of Chemistry, National Institute of Technology, Tiruchirappalli, Tamil Nadu 620015, India*

Nidhi Anilkumar Jamuna − *Department of Chemistry, National Institute of Technology, Tiruchirappalli, Tamil Nadu 620015, India*

Roselin Ansilda − *Department of Chemistry, National Institute of Technology, Tiruchirappalli, Tamil Nadu 620015, India*

Complete contact information is available at: https://pubs.acs.org/10.1021/acsomega.2c00839

Notes

The authors declare no competing financial interest.

■ ACKNOWLEDGMENTS

S.M. is thankful to the Science and Engineering Research Board (SERB), Government of India, for a Start-up Research Grant (SRG) and Department of Science and Technology, Government of India, for an INSPIRE-Faculty Research Grant. A.M.C.D. is thankful to SERB for a research fellowship. A.K. and A.J.N. are thankful to the National Institute of Technology Tiruchirappalli for a research fellowship. R.A. is thankful to DST for a research fellowship.

■ REFERENCES

(1) Lee, C.; Wei, X.; Kysar, J. W.; Hone, J. J. s. Measurement of the elastic properties and intrinsic strength of monolayer graphene. *Science* **2008**, *321*, 385−388.

(2) Balandin, A. A.; Ghosh, S.; Bao, W.; Calizo, I.; Teweldebrhan, D.; Miao, F.; Lau, C. N. Superior Thermal Conductivity of Single-Layer Graphene. *Nano Lett.* **2008**, *8*, 902−907.

(3) Castro Neto, A. H.; Guinea, F.; Peres, N. M. R.; Novoselov, K. S.; Geim, A. K. The electronic properties of graphene. *Rev. Mod. Phys.* **2009**, *81*, 109−162.

(4) Avouris, P. Graphene: electronic and photonic properties and devices. *Nano Lett.* **2010**, *10*, 4285−4294.

(5) Xu, M.; Liang, T.; Shi, M.; Chen, H. Graphene-Like Two-Dimensional Materials. *Chem. Rev.* **2013**, *113*, 3766−3798.
(6) Bolotsky, A.; Butler, D.; Dong, C.; Gerace, K.; Glavin, N. R.; Muratore, C.; Robinson, J. A.; Ebrahimi, A. Two-Dimensional Materials in Biosensing and Healthcare: From In Vitro Diagnostics to Optogenetics and Beyond. *ACS Nano* **2019**, *13*, 9781−9810.
(7) Zhu, C.; Du, D.; Lin, Y. Graphene and graphene-like 2D materials for optical biosensing and bioimaging: a review. *2D Mater.* **2015**, *2*, No. 032004.
(8) Politano, A.; Chiarello, G.; Spinella, C. Plasmon spectroscopy of graphene and other two-dimensional materials with transmission electron microscopy. *Mater. Sci. Semicond. Process.* **2017**, *65*, 88−99.
(9) Dhakal, K. P.; Duong, D. L.; Lee, J.; Nam, H.; Kim, M.; Kan, M.; Lee, Y. H.; Kim, J. Confocal absorption spectral imaging of MoS2: optical transitions depending on the atomic thickness of intrinsic and chemically doped MoS2. *Nanoscale* **2014**, *6*, 13028−13035.
(10) Gupta, A.; Arunachalam, V.; Vasudevan, S. Water Dispersible, Positively and Negatively Charged MoS2 Nanosheets: Surface Chemistry and the Role of Surfactant Binding. *J. Phys. Chem. Lett.* **2015**, *6*, 739−744.
(11) Li, X.; Zhu, H. Two-dimensional MoS2: Properties, preparation, and applications. *Journal of Materiomics* **2015**, *1*, 33−44.
(12) Barua, S.; Dutta, H. S.; Gogoi, S.; Devi, R.; Khan, R. Nanostructured MoS2-Based Advanced Biosensors: A Review. *ACS Appl. Nano Mater.* **2018**, *1*, 2−25.
(13) Nourbakhsh, A.; Zubair, A.; Sajjad, R. N.; Tavakkoli, K. G. A.; Chen, W.; Fang, S.; Ling, X.; Kong, J.; Dresselhaus, M. S.; Kaxiras, E.; Berggren, K. K.; Antoniadis, D.; Palacios, T. MoS2 Field-Effect Transistor with Sub-10 nm Channel Length. *Nano Lett.* **2016**, *16*, 7798−7806.
(14) Deng, Y.; Luo, Z.; Conrad, N. J.; Liu, H.; Gong, Y.; Najmaei, S.; Ajayan, P. M.; Lou, J.; Xu, X.; Ye, P. D. Black Phosphorus−Monolayer MoS2 van der Waals Heterojunction p−n Diode. *ACS Nano* **2014**, *8*, 8292−8299.
(15) Ali, A.; Mangrio, F. A.; Chen, X.; Dai, Y.; Chen, K.; Xu, X.; Xia, R.; Zhu, L. Ultrathin MoS2 nanosheets for high-performance photoelectrochemical applications via plasmonic coupling with Au nanocrystals. *Nanoscale* **2019**, *11*, 7813−7824.
(16) Bhatnagar, M.; Gardella, M.; Giordano, M. C.; Chowdhury, D.; Mennucci, C.; Mazzanti, A.; Valle, G. D.; Martella, C.; Tummala, P.; Lamperti, A.; Molle, A.; Buatier de Mongeot, F. Broadband and Tunable Light Harvesting in Nanorippled MoS2 Ultrathin Films. *ACS Appl. Mater. Interfaces* **2021**, *13*, 13508−13516.
(17) Yang, H.; Liu, Y.; Gao, C.; Meng, L.; Liu, Y.; Tang, X.; Ye, H. Adsorption Behavior of Nucleobases on Doped MoS2Monolayer: A DFT Study. *J. Phys. Chem. C* **2019**, *123*, 30949−30957.
(18) Kaur, J.; Singh, M.; Dell Aversana, C.; Benedetti, R.; Giardina, P.; Rossi, M.; Valadan, M.; Vergara, A.; Cutarelli, A.; Montone, A. M. I.; Altucci, L.; Corrado, F.; Nebbioso, A.; Altucci, C. Biological interactions of biocompatible and water-dispersed MoS2 nanosheets with bacteria and human cells. *Sci. Rep.* **2018**, *8*, 16386.
(19) Laursen, A. B.; Kegnæs, S.; Dahl, S.; Chorkendorff, I. Molybdenum sulfides—efficient and viable materials for electro - and photoelectrocatalytic hydrogen evolution. *Energy Environ. Sci.* **2012**, *5*, 5577−5591.
(20) Akhtar, M. A.; Batool, R.; Hayat, A.; Han, D.; Riaz, S.; Khan, S. U.; Nasir, M.; Nawaz, M. H.; Niu, L. Functionalized Graphene Oxide Bridging between Enzyme and Au-Sputtered Screen-Printed Interface for Glucose Detection. *ACS Appl. Nano Mater.* **2019**, *2*, 1589−1596.
(21) Lee, J.; Dak, P.; Lee, Y.; Park, H.; Choi, W.; Alam, M. A.; Kim, S. Two-dimensional Layered MoS2 Biosensors Enable Highly Sensitive Detection of Biomolecules. *Sci. Rep.* **2014**, *4*, 7352.
(22) Sheldon, R. A.; van Pelt, S. Enzyme immobilisation in biocatalysis: why, what and how. *Chem. Soc. Rev.* **2013**, *42*, 6223−6235.
(23) Roach, P.; Farrar, D.; Perry, C. C. Surface Tailoring for Controlled Protein Adsorption: Effect of Topography at the Nanometer Scale and Chemistry. *J. Am. Chem. Soc.* **2006**, *128*, 3939−3945.
(24) Gupta, A.; Vasudevan, S. Understanding Surfactant Stabilization of MoS2 Nanosheets in Aqueous Dispersions from Zeta Potential Measurements and Molecular Dynamics Simulations. *J. Phys. Chem. C* **2018**, *122*, 19243−19250.
(25) Yu, J.; Ma, D.; Mei, L.; Gao, Q.; Yin, W.; Zhang, X.; Yan, L.; Gu, Z.; Ma, X.; Zhao, Y. Peroxidase-like activity of MoS2 nanoflakes with different modifications and their application for H2O2 and glucose detection. *J. Mater. Chem. B* **2018**, *6*, 487−498.
(26) Suthiwangcharoen, N.; Nagarajan, R. Enhancing Enzyme Stability by Construction of Polymer−Enzyme Conjugate Micelles for Decontamination of Organophosphate Agents. *Biomacromolecules* **2014**, *15*, 1142−1152.
(27) Alexandridis, P.; Tsianou, M. Block copolymer-directed metal nanoparticle morphogenesis and organization. *Eur. Polym. J.* **2011**, *47*, 569−583.
(28) Rahme, K.; Gauffre, F.; Marty, J.-D.; Payré, B.; Mingotaud, C. A Systematic Study of the Stabilization in Water of Gold Nanoparticles by Poly(Ethylene Oxide)−Poly(Propylene Oxide)−Poly(Ethylene Oxide) Triblock Copolymers. *J. Phys. Chem. C* **2007**, *111*, 7273−7279.
(29) Kundu, N.; Roy, A.; Banik, D.; Kuchlyan, J.; Sarkar, N. Graphene Oxide and Pluronic Copolymer Aggregates−Possible Route to Modulate the Adsorption of Fluorophores and Imaging of Live Cells. *J. Phys. Chem. C* **2015**, *119*, 25023−25035.
(30) Fernandes, R. M. F.; Dai, J.; Regev, O.; Marques, E. F.; Furó, I. Block Copolymers as Dispersants for Single-Walled Carbon Nanotubes: Modes of Surface Attachment and Role of Block Polydispersity. *Langmuir* **2018**, *34*, 13672−13679.
(31) Jiang, X.; Wang, X. Cytochrome C-Mediated Apoptosis. *Annu. Rev. Biochem.* **2004**, *73*, 87−106.
(32) Tarpani, L.; Bellezza, F.; Sassi, P.; Gambucci, M.; Cipiciani, A.; Latterini, L. New Insights into the Effects of Surface Functionalization on the Peroxidase Activity of Cytochrome c Adsorbed on Silica Nanoparticles. *J. Phys. Chem. B* **2019**, *123*, 2567−2575.
(33) Bushnell, G. W.; Louie, G. V.; Brayer, G. D. High-resolution three-dimensional structure of horse heart cytochrome c. *J. Mol. Biol.* **1990**, *214*, 585−595.
(34) Yin, V.; Shaw, G. S.; Konermann, L. Cytochrome c as a Peroxidase: Activation of the Precatalytic Native State by H2O2-Induced Covalent Modifications. *J. Am. Chem. Soc.* **2017**, *139*, 15701−15709.
(35) Belikova, N. A.; Vladimirov, Y. A.; Osipov, A. N.; Kapralov, A. A.; Tyurin, V. A.; Potapovich, M. V.; Basova, L. V.; Peterson, J.; Kurnikov, I. V.; Kagan, V. E. Peroxidase Activity and Structural Transitions of Cytochrome c Bound to Cardiolipin-Containing Membranes. *Biochemistry* **2006**, *45*, 4998−5009.
(36) Mandal, A.; Hoop, C. L.; DeLucia, M.; Kodali, R.; Kagan, V. E.; Ahn, J.; van der Wel, P. C. A. Structural Changes and Proapoptotic Peroxidase Activity of Cardiolipin-Bound Mitochondrial Cytochrome c. *Biophys. J.* **2015**, *109*, 1873−1884.
(37) Veitch, N. C. Horseradish peroxidase: a modern view of a classic enzyme. *Phytochemistry* **2004**, *65*, 249−259.
(38) Benson, K. R.; Gorecki, J.; Nikiforov, A.; Tsui, W.; Kasi, R. M.; Kumar, C. V. Cytochrome c-poly(acrylic acid) conjugates with improved peroxidase turnover number. *Org. Biomol. Chem.* **2019**, *17*, 4043−4048.
(39) Wu, L.; Jiang, X. Enhancing Peroxidase Activity of Cytochrome c by Modulating Interfacial Interaction Forces with Graphene Oxide. *Langmuir* **2020**, *36*, 1094−1102.
(40) Yang, X.; Zhao, C.; Ju, E.; Ren, J.; Qu, X. Contrasting modulation of enzyme activity exhibited by graphene oxide and reduced graphene. *Chem. Commun.* **2013**, *49*, 8611−8613.
(41) Chen, Y.; Jiménez-Ángeles, F.; Qiao, B.; Krzyaniak, M. D.; Sha, F.; Kato, S.; Gong, X.; Buru, C. T.; Chen, Z.; Zhang, X.; Gianneschi, N. C.; Wasielewski, M. R.; Olvera de la Cruz, M.; Farha, O. K. Insights into the Enhanced Catalytic Activity of Cytochrome c When Encapsulated in a Metal−Organic Framework. *J. Am. Chem. Soc.* **2020**, *142*, 18576−18582.

https://doi.org/10.1021/acsomega.2c00839
ACS Omega 2022, 7, 16593−16604

(42) Essner, J. B.; McCay, R. N.; Smith Ii, C. J.; Cobb, S. M.; Laber, C. H.; Baker, G. A. A switchable peroxidase mimic derived from the reversible co-assembly of cytochrome c and carbon dots. *J. Mater. Chem. B* **2016**, *4*, 2163−2170.
(43) Quinn, M. D. J.; Ho, N. H.; Notley, S. M. Aqueous Dispersions of Exfoliated Molybdenum Disulfide for Use in Visible-Light Photocatalysis. *ACS Appl. Mater. Interfaces* **2013**, *5*, 12751−12756.
(44) Varrla, E.; Backes, C.; Paton, K. R.; Harvey, A.; Gholamvand, Z.; McCauley, J.; Coleman, J. N. Large-Scale Production of Size-Controlled MoS2 Nanosheets by Shear Exfoliation. *Chem. Mater.* **2015**, *27*, 1129−1139.
(45) Wang, K.; Wang, J.; Fan, J.; Lotya, M.; O'Neill, A.; Fox, D.; Feng, Y.; Zhang, X.; Jiang, B.; Zhao, Q.; Zhang, H.; Coleman, J. N.; Zhang, L.; Blau, W. J. Ultrafast Saturable Absorption of Two-Dimensional MoS2 Nanosheets. *ACS Nano* **2013**, *7*, 9260−9267.
(46) Pešić, J.; Vujin, J.; Tomašević-Ilić, T.; Spasenović, M.; Gajić, R. DFT study of optical properties of MoS2 and WS2 compared to spectroscopic results on liquid phase exfoliated nanoflakes. *Opt. Quantum Electron.* **2018**, *50*, 291.
(47) Ghayeb Zamharir, S.; Karimzadeh, R.; Aboutalebi, S. H. Laser-assisted tunable optical nonlinearity in liquid-phase exfoliated MoS2 dispersion. *Appl. Phys. A: Mater. Sci. Process.* **2018**, *124*, 692.
(48) Su, Y.-l.; Wang, J.; Liu, H.-z. Formation of a Hydrophobic Microenvironment in Aqueous PEO−PPO−PEO Block Copolymer Solutions Investigated by Fourier Transform Infrared Spectroscopy. *J. Phys. Chem. B* **2002**, *106*, 11823−11828.
(49) Feng, W.; Chen, L.; Qin, M.; Zhou, X.; Zhang, Q.; Miao, Y.; Qiu, K.; Zhang, Y.; He, C. Flower-like PEGylated MoS2 nanoflakes for near-infrared photothermal cancer therapy. *Sci. Rep.* **2015**, *5*, 17422.
(50) Parray, Z. A.; Ahmad, F.; Alajmi, M. F.; Hussain, A.; Hassan, M. I.; Islam, A. Interaction of polyethylene glycol with cytochrome c investigated via in vitro and in silico approaches. *Sci. Rep.* **2021**, *11*, 6475.
(51) Ye, M.; Zhang, Q.-L.; Li, H.; Weng, Y.-X.; Wang, W.-C.; Qiu, X.-G. Infrared Spectroscopic Discrimination between the Loop and α-Helices and Determination of the Loop Diffusion Kinetics by Temperature-Jump Time-Resolved Infrared Spectroscopy for Cytochrome c. *Biophys. J.* **2007**, *93*, 2756−2766.
(52) Gao, H.; Zhao, J.; Huang, Y.; Cheng, X.; Wang, S.; Han, Y.; Xiao, Y.; Lou, X. Universal Design of Structure-Switching Aptamers with Signal Reporting Functionality. *Anal. Chem.* **2019**, *91*, 14514−14521.
(53) Song, Y.; Qu, K.; Zhao, C.; Ren, J.; Qu, X. Graphene oxide: intrinsic peroxidase catalytic activity and its application to glucose detection. *Adv. Mater.* **2010**, *22*, 2206−2210.
(54) Wang, L.; Waldeck, D. H. Denaturation of Cytochrome c and Its Peroxidase Activity When Immobilized on SAM Films. *J. Phys. Chem. C* **2008**, *112*, 1351−1356.
(55) Gao, L. Z.; Zhuang, J.; Nie, L.; Zhang, J. B.; Zhang, Y.; Gu, N.; Wang, T. H.; Feng, J.; Yang, D. L.; Perrett, S.; Yan, X. Intrinsic peroxidase-like activity of ferromagnetic nanoparticles. *Nat. Nanotechnol.* **2007**, *2*, 577−583.
(56) Rodriguez-Lopez, J. N.; Gilabert, M. A.; Tudela, J.; Thorneley, R. N.; Garcia-Canovas, F. Reactivity of horseradish peroxidase compound II toward substrates: kinetic evidence for a two-step mechanism. *Biochemistry* **2000**, *39*, 13201−13209.
(57) Ghosh, A.; Mitchell, D. A.; Chanda, A.; Ryabov, A. D.; Popescu, D. L.; Upham, E. C.; Collins, G. J.; Collins, T. J. Catalase-Peroxidase Activity of Iron(III)-TAML Activators of Hydrogen Peroxide. *J. Am. Chem. Soc.* **2008**, *130*, 15116−15126.
(58) Blackmond, D. G. Reaction progress kinetic analysis: a powerful methodology for mechanistic studies of complex catalytic reactions. *Angew. Chem., Int. Ed.* **2005**, *44*, 4302−4320.
(59) Bures, J. A Simple Graphical Method to Determine the Order in Catalyst. *Angew. Chem., Int. Ed.* **2016**, *55*, 2028−2031.

https://doi.org/10.1021/acsomega.2c00839
ACS Omega 2022, 7, 16593−16604